Thermal transport through a spin-phonon interacting junction: A nonequilibrium Green's function method study

Zu-Quan Zhang and Jing-Tao Lü*

School of Physics and Wuhan National High Magnetic Field Center, Huazhong University of Science and Technology, 430074 Wuhan, People's Republic of China

(Received 12 July 2017; published 21 September 2017)

Using the nonequilibrium Green's function method, we consider heat transport in an insulating ferromagnetic spin chain model with spin-phonon interaction under an external magnetic field. Employing the Holstein-Primakoff transformation to the spin system, we treat the resulted magnon-phonon interaction within the self-consistent Born approximation. We find the magnon-phonon coupling can change qualitatively the magnon thermal conductance in the high-temperature regime. At a spectral mismatched ferromagnetic-normal insulator interface, we also find thermal rectification and negative differential thermal conductance due to the magnon-phonon interaction. We show that these effects can be effectively tuned by the external applied magnetic field, a convenient advantage absent in anharmonic phonon and electron-phonon systems studied before.

DOI: 10.1103/PhysRevB.96.125432

I. INTRODUCTION

Recently, the study of heat transport carried by spin degrees of freedom has received widespread interest, and it has created the field of spin caloritronics [1]. One notable example is the spin Seebeck effect [2,3] (SSE), in which the application of a temperature gradient drives a spin current. With the rapid progress in the experiments, the SSE has been discovered in different types of materials in different experimental setups [2–7].

Further investigation [8–14] suggests that spin-phonon interaction plays a vital role in the SSE. In the acoustic spin-pumping experiment [10–12], a three-layer hybrid structure of a nonmagnetic metal, a ferromagnetic insulator, and a piezoelectric actuator of a normal insulator is used to pump spin using acoustic waves generated in the piezoelectric actuator. In the ferromagnetic-normal (FN) insulator interface, a key process is the energy transfer from the normal insulator to the ferromagnetic insulator through spin-phonon interaction. This experiment not only provides a new way of spin-pumping by directly injecting sound waves, but it also gives a persuasive explanation of phonon-mediated spin-pumping to the long-range feature of the SSE in different materials. A theoretical approach of the phonon-drag mechanism shows a proportional relationship between acoustic spin-pumping and the power of an external sound wave [12].

Motivated by the rapid progress, several authors studied spin transport in various nanojunction models [15–17]. A typical junction of this type is formed by quantum dots bridging metal and ferromagnetic insulator leads [17]. The main energy carriers are electrons in the metal lead and spin waves in the ferromagnetic insulator lead. They exchange energy at the quantum dot through exchange coupling. Energy transport in the linear and nonlinear regimes is studied. Following a similar idea, we study the influence of spin-phonon interaction on the thermal transport of a junction considering both spin and phonon degrees of freedom. A Heisenberg model is used to describe the magnetic exchange interaction, and a harmonic-oscillator model is used to describe the phonons. The spin-phonon interaction is introduced in terms of the Su-Schrieffer-Heeger (SSH) -like model [18] in the junction. First, following a Holstein-Primakoff transformation, we discuss the temperature dependence of the thermal conductances contributed by magnon and phonon degrees of freedom in the junction, and we analyze their dependence on the spin-phonon interaction. Second, we show that thermal rectification (TR) and negative differential thermal conductance (NDTC) show up in the junction, whose mechanism is different from other similar setups using electron-phonon or anharmonic phonon couplings [19–21], and they can be controlled by an external magnetic field. We further discuss the influence of different transport processes on these two effects.

II. MODEL AND METHOD

The model system is a one-dimensional (1D) insulating ferromagnetic spin junction under a uniform external magnetic field, as shown in Fig. 1. The leads are modeled by two semi-infinite chains, which are in their thermal equilibrium with well-defined temperatures. The center part lies between the two leads. We assume that the spin-phonon interaction only takes place in the center region. The Hamiltonian of the whole system is divided into three parts:

$$H = H_J + H_{\rm ph} + H_{\rm int}, \tag{1}$$

i.e., the Heisenberg spin Hamiltonian H_J, the phonon Hamiltonian $H_{\rm ph}$, and their interaction $H_{\rm int}$. The spin part is written as

$$H_{\rm J} = -\frac{1}{2}\sum_{\alpha,\beta=L,R,C}\sum_{|i-j|=1} J_{ij}^{\alpha\beta}\boldsymbol{S}_i^{\alpha}\cdot\boldsymbol{S}_j^{\beta} - h_z\sum_i S_i^z, \tag{2}$$

where we only consider the nearest-neighbor exchange interaction. For simplicity, we use J_{ij}^{α} if α and β belong to the same region, as for the dynamic matrix below. The magnetic field is chosen to be along the z direction denoted by h_z. Under the

*jtlu@hust.edu.cn

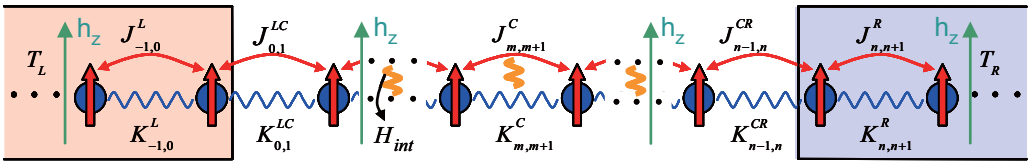

FIG. 1. Model diagram of a 1D insulating ferromagnetic spin junction under an external magnetic field. Spin-phonon interaction is included only in the central region. The two leads are modeled by semi-infinite chains with different temperatures.

harmonic approximation, the phonon Hamiltonian is [22,23]

$$H_{\rm ph}=\frac{1}{2}\sum_{\alpha,i}\left(\dot{u}_i^{\alpha}\dot{u}_i^{\alpha}+u_i^{\alpha}K_{ii}^{\alpha}u_i^{\alpha}\right)+\frac{1}{2}\sum_{\alpha\beta}\sum_{|i-j|=1}u_i^{\alpha}K_{ij}^{\alpha\beta}u_j^{\beta}, \tag{3}$$

where $\dot{u}_i^{\alpha}=p_i^{\alpha}/\sqrt{m_i^{\alpha}}$ and $u_i^{\alpha}=\sqrt{m_i^{\alpha}}r_i^{\alpha}$. Here $p_i^{\alpha},r_i^{\alpha}$ are the momentum and displacement operators of atom i in region α, respectively, m_i^{α} is the atom mass, and $K_{ii}^{\alpha},K_{ij}^{\alpha\beta}$ are elements of the dynamical matrix.

The spin-phonon interaction is introduced through the SSH-like model in the central region. The nearest-neighbor exchange interaction is expanded to first order with respect to the mass renormalized displacements from equilibrium positions,

$$\mathcal{J}_{ij}^{C}=J_{ij}^{C}+\lambda_{ij}\left(u_i^{C}-u_j^{C}\right), \tag{4}$$

where J_{ij}^{C} is the exchange interaction with the atoms in their equilibrium positions, and $\lambda_{ij}=(d\mathcal{J}_{ij}^{C}/du_i^{C})_{u_i^{C}=0}$. We note that $\mathcal{J}_{ij}^{C}$ increases with the reducing of the neighbor atom distance while it decreases with the increasing of it. This is reflected by the relation $\lambda_{ij}=-\lambda_{ji}$. Thus, the interaction Hamiltonian in the central region is given by

$$H_{\rm int}=-\frac{1}{2}\sum_{\langle ij\rangle}\lambda_{ij}\left(u_i^{C}-u_j^{C}\right)\boldsymbol{S}_i^{C}\cdot\boldsymbol{S}_j^{C}. \tag{5}$$

To treat the spin-phonon interaction, we map the spin operators to bosonic operators (magnons) by the approximated Holstein-Primakoff transformation [24]:

$$S_i^{+}\approx\sqrt{2\bar{S}_i}a_i, \tag{6a}$$

$$S_i^{-}\approx\sqrt{2\bar{S}_i}a_i^{\dagger}, \tag{6b}$$

$$S_i^{z}\approx\bar{S}_i-a_i^{\dagger}a_i. \tag{6c}$$

Here, $a_i^{\dagger}$ (a_i) is the magnon creation (annihilation) operator at site i, and $\bar{S}_i$ is the average of the spin at site i. The magnon approximation is valid when the local spins are near their parallel aligned ground states, i.e., the local magnon occupation number is small, $\langle a_i^{\dagger}a_i\rangle\ll\bar{S}_i$. We use $\bar{S}=10$ for all regions in this paper. Under this approximation, neglecting the constant terms that do not contribute to the energy transport, we write Eqs. (2) and (5) as

$$H_J\approx\sum_{|i-j|=0,1}\sum_{\alpha,\beta}a_i^{\dagger\alpha}X_{ij}^{\alpha\beta}a_j^{\beta}, \tag{7}$$

$$H_{\rm int}\approx\sum_{|i-j|=0,1}\sum_{k}M_{ij}^{k}a_i^{\dagger C}a_j^{C}u_k^{C}, \tag{8}$$

where $X_{ii}^{\alpha}=\sum_{\delta}J_{i,i+\delta}^{\alpha\beta}\bar{S}_{i+\delta}^{\beta}+h_z$ and $X_{ij}^{\alpha\beta}=-J_{ij}^{\alpha\beta}\sqrt{\bar{S}_i^{\alpha}\bar{S}_j^{\beta}}$ $(i\neq j)$. The magnon-phonon coupling matrix is $M_{ii}^{k}=\sum_{\delta}\lambda_{i,i+\delta}\bar{S}_{i+\delta}^{C}(\delta_{ki}-\delta_{k,i+\delta})$ and $M_{ij}^{k}=-\lambda_{ij}\sqrt{\bar{S}_i^{C}\bar{S}_j^{C}}(\delta_{ki}-\delta_{kj})(i\neq j)$. The simplified Hamiltonian is similar to that of the electron-phonon case [22], and it can be solved similarly.

We calculate the transport properties of the systems by using the NEGF technique [25,26], which was applied recently to the coupling systems with electron-phonon interaction [22,27–30] and electron-magnon interaction [31] under the self-consistent Born approximation (SCBA). Here it is used to deal with the magnon-phonon interaction.

First, we solve the Green's functions (GFs) without magnon-phonon interaction. The retarded GF for magnons is $G_0^{r}(\varepsilon)=[(\varepsilon+i\eta)\mathbb{1}-X^{C}-\Sigma_{\rm leads}^{r}(\varepsilon)]^{-1}$, with $\mathbb{1}$ being the identity matrix, and X^{C} is the Hamiltonian matrix for the central region from Eq. (7). $\Sigma_{\rm leads}^{r}(\varepsilon)$ is the lead's self-energy matrix and diagonal in our case. $\Sigma_{\alpha}^{r}=X^{C\alpha}g_{\alpha}^{r}X^{\alpha C}$ is for coupling to lead α, where g_{α}^{r} is the surface GF of lead α for magnons. For steady-state transport, the lesser GF is given by the Keldysh equation $G_0^{<}=G_0^{r}\Sigma_{\rm leads}^{<}G_0^{a}$, with $\Sigma_{\alpha}^{<}=f_{\alpha}^{B}(\Sigma_{\alpha}^{r}-\Sigma_{\alpha}^{a})$. f_{α}^{B} is the Bose distribution function for lead α. The relation $G_0^{a}(\varepsilon)=[G_0^{r}(\varepsilon)]^{\dagger}$, $\Sigma_{\rm leads}^{a}(\varepsilon)=[\Sigma_{\rm leads}^{r}(\varepsilon)]^{\dagger}$ is used for getting the advanced GF or self-energy from retarded ones, and it will also be used in the following text. Similarly for phonons, the retarded GF is $D_0^{r}(\omega)=[(\omega+i\eta)^2\mathbb{1}-K^{C}-\Pi_{\rm leads}^{r}(\omega)]^{-1}$, where K^{C} is the dynamical matrix for the central region in Eq. (3). Phonon self-energy due to lead α is $\Pi_{\alpha}^{r}=K^{C\alpha}d_{\alpha}^{r}K^{\alpha C}$, where d_{α}^{r} is the lead's surface GF for phonons. The lesser GF is $D_0^{<}=D_0^{r}\Pi_{\rm leads}^{<}D_0^{a}$, with $\Pi_{\alpha}^{<}=f_{\alpha}^{B}(\Pi_{\alpha}^{r}-\Pi_{\alpha}^{a})$.

Secondly, taking the magnon-phonon interaction as a perturbation to the noninteracting magnon and phonon GFs, the full GF can be solved by the Dyson equation. For magnons, it is given by $G^{r}=G_0^{r}+G_0^{r}\Sigma_{\rm SCBA}^{r}G^{r}$, and the Keldysh equation is $G^{<}=G^{r}\Sigma_{\rm tot}^{<}G^{a}$. Here $\Sigma_{\rm tot}^{<}=\Sigma_{\rm leads}^{<}+\Sigma_{\rm SCBA}^{<}$ is the total self-energy. Similarly for phonons, we have $D^{r}=D_0^{r}+D_0^{r}\Pi_{\rm SCBA}^{r}D^{r}$, $D^{<}=D^{r}\Pi_{\rm tot}^{<}D^{a}$, and $\Pi_{\rm tot}^{<}=\Pi_{\rm leads}^{<}+\Pi_{\rm SCBA}^{<}$. Diagram representations for the self-energies under SCBA are shown in Fig. 2. Different from that of the electron-phonon case [22,30], despite the similarity, the bosonic loops of magnons in the Hartree and polarization-like diagrams do not gain a minus sign here. The retarded Hartree self-energy is

$$\Sigma_{mn}^{H,r}=i\hbar M_{mn}^{i}D_{0,ij}^{r}(\omega'=0)M_{kl}^{j}\int\frac{d\varepsilon}{2\pi\hbar}G_{lk}^{<}(\varepsilon). \tag{9}$$

The Fock self-energies are

$$\Sigma_{mn}^{F,<}(\varepsilon)=i\hbar\int\frac{d\omega}{2\pi}M_{mi}^{k}G_{ij}^{<}(\varepsilon-\hbar\omega)D_{kl}^{<}(\omega)M_{jn}^{l} \tag{10}$$

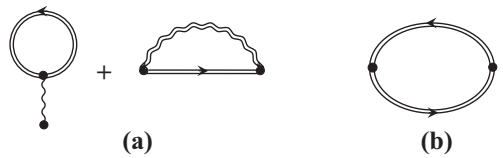

FIG. 2. Diagram representations for the self-energies of (a) magnons and (b) phonons under the SCBA. The double wavy line and single wavy line are for the full and noninteracting GFs of phonons, respectively. The double straight line is for the full GF of magnons.

and

$$\Sigma^{F,r}_{mn}(\varepsilon) = i\hbar \int \frac{d\omega}{2\pi} M^k_{mi} \{ G^<_{ij}(\varepsilon - \hbar\omega) D^r_{kl}(\omega) + G^r_{ij}(\varepsilon - \hbar\omega) \left[D^<_{kl}(\omega) + D^r_{kl}(\omega) \right] \} M^l_{jn}. \quad (11)$$

We have $\Sigma^r_{\rm SCBA}(\varepsilon) = \Sigma^{F,r}(\varepsilon) + \Sigma^{H,r}(\varepsilon)$ and $\Sigma^<_{\rm SCBA}(\varepsilon) = \Sigma^{F,<}(\varepsilon)$. The polarization-like self-energies are

$$[\Pi^<_{\rm SCBA}]_{mn}(\omega) = i\hbar \int \frac{d\varepsilon}{2\pi\hbar} M^m_{lk} G^<_{ki}(\varepsilon) G^>_{jl}(\varepsilon - \hbar\omega) M^n_{ij}, \quad (12)$$

$$\left[\Pi^r_{\rm SCBA}\right]_{mn}(\omega) = i\hbar \int \frac{d\varepsilon}{2\pi\hbar} M^m_{lk} \left[G^r_{ki}(\varepsilon) G^<_{jl}(\varepsilon - \hbar\omega) + G^<_{ki}(\varepsilon) G^a_{jl}(\varepsilon - \hbar\omega) \right] M^n_{ij}. \quad (13)$$

The full GFs and the self-energies need to be solved self-consistently.

The energy current of magnons flowing out of lead α is expressed in terms of the Meir-Wingreen formula [32,33] as

$$I^{\rm J}_\alpha = -\frac{1}{\hbar} \int \frac{d\varepsilon}{2\pi} \varepsilon \, {\rm Tr}[G^>(\varepsilon)\Sigma^<_\alpha(\varepsilon) - G^<(\varepsilon)\Sigma^>_\alpha(\varepsilon)]. \quad (14)$$

Similarly, the energy current of phonons is

$$I^{\rm ph}_\alpha = -\frac{1}{2} \int \frac{d\omega}{2\pi} \hbar\omega \, {\rm Tr}[D^>(\omega)\Pi^<_\alpha(\omega) - D^<(\omega)\Pi^>_\alpha(\omega)]. \quad (15)$$

Here, the integrals are from $-\infty$ to $+\infty$. The total energy current flowing out of lead α is their summation, i.e., $I_\alpha = I^J_\alpha + I^{\rm ph}_\alpha$. The energy current from magnons to phonons is $I_{J\to{\rm ph}} = I^J_L + I^J_R$, and that from phonons to magnons is $I_{{\rm ph}\to J} = I^{\rm ph}_L + I^{\rm ph}_R$. It can be shown that the SCBA conserves energy, which is reflected by the relation $I_{J\to{\rm ph}} + I_{{\rm ph}\to J} = 0$.

III. NUMERIC RESULTS AND DISCUSSION

As applications of the above theory, we consider the case of two atomic sites as the central region connecting to two leads. These two sites can also be considered as two quantum dots. The parameters of the two leads are set to be the same. The magnon-phonon coupling strength is set as $|M^k_{ij}| = M_0 (i,j,k = 1,2)$. The exchange parameters, the external magnetic field, the dynamical matrix, and the magnon-phonon coupling are all converted to energy for convenience. All calculations are done within the SCBA. A cutoff energy of 2 eV is used throughout.

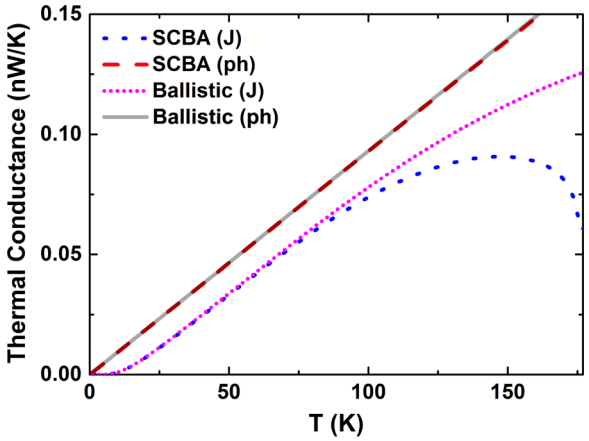

FIG. 3. Thermal conductances of the 1D ferromagnetic Heisenberg junction for magnons and phonons under an external magnetic field. Parameters of the central region are $J^C_{12} = 1.5$ meV, $K^C_{12} = 6 \times 10^4$ meV^2. For the leads, J^L_{ij} and J^R_{ij} are 2 meV; K^L_{ij} and K^R_{ij} are 1×10^5 meV^2. Couplings of the central region with the leads are $J^{LC}_{01} = J^{CR}_{23} = J^C_{12}$, $K^{LC}_{01} = K^{CR}_{23} = K^C_{12}$. The magnon-phonon coupling constant is $M_0 = 14$ meV. The external magnetic field is $h_z = 4$ meV for all regions.

A. Thermal conductance in a junction with magnon-phonon interaction

We show in Fig. 3 the thermal conductances of magnons and phonons in a ferromagnetic junction under an external magnetic field. Their summation gives the total thermal conductance. To calculate the thermal conductance, we choose a very small temperature difference between the two leads. The thermal conductance is calculated from the thermal current and temperature difference as $\kappa^i = |I^i/\Delta T|$ $(i = J, {\rm ph})$.

We can see in Fig. 3 that the phonon thermal conductance shows little change with or without the magnon-phonon interaction. The very limited influence of the magnon-phonon coupling to the phonon thermal transport is mainly due to the magnetic field h_z here, which "freezes" the low-energy magnons and makes the magnons less populated in the temperature range considered. However, the thermal conductance contributed by magnons is affected by the magnon-phonon interaction at high temperature. It shows a peak at a temperature about 140 K, and decreases upon further increase of the temperature. This phenomenon is absent in the ballistic case. This peak is also observable in the total thermal conductance of the junction, and it can be considered as a signature of the magnon-mediated thermal transport.

In the low-temperature region, the magnon-phonon interaction is suppressed. The thermal conductance of the phonons and magnons shows ballistic behavior. But they have quite different temperature dependences. The former shows a linear temperature dependence, while the latter dependence is exponential. This can be understood from a one-dimensional chain with translational invariance, neglecting the magnon-phonon interaction. In this case, the temperature dependences of thermal conductance contributed by magnons and phonons are given, respectively, as (see Appendix) $\kappa^J \propto \frac{1}{T} \exp[-\frac{h_z}{k_B T}]$ and $\kappa^{\rm ph} \propto T$, where k_B is the Boltzmann constant. We see clearly that the external magnetic field "freezes" the thermal

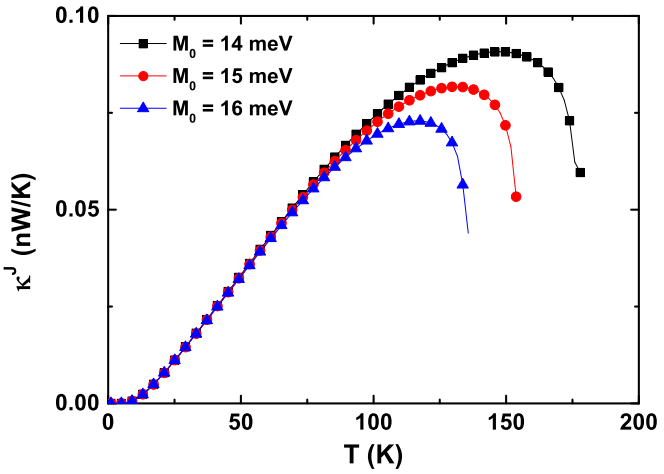

FIG. 4. Thermal conductance for the magnons with different magnon-phonon coupling constants. The other parameters are the same as those in Fig. 3.

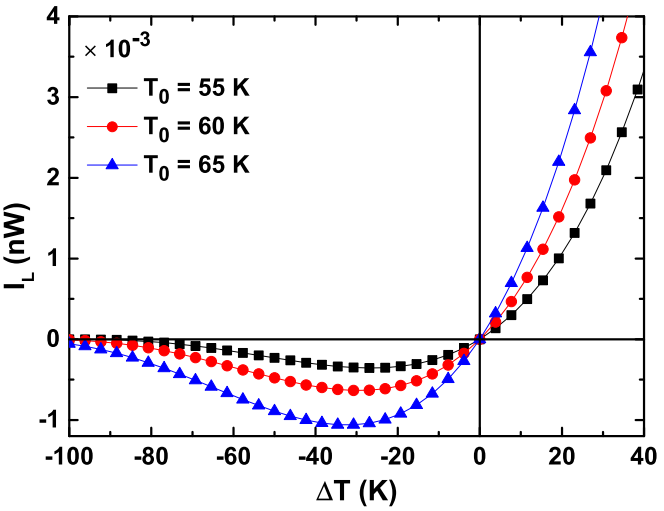

FIG. 5. Energy current I_L of an FN insulator interface device as a function of the temperature bias ΔT with $T_{L,R} = T_0 \pm \Delta T/2$. T_0 is the average temperature of the two electrodes. The strength of Heisenberg ferromagnetic exchange interactions is 2 meV for all the regions on the left side of atom 2 in Fig. 1, and they are effectively zero in the right region. The magnitude of the dynamic matrix elements is $K_0 = 1 \times 10^5$ meV^2 for all the regions on the right side of atom 1, and they are very large for its left region. The magnon-phonon coupling strength is $M_0 = 20$ meV. The external magnetic field is $h_z = 2$ meV for the magnetic part.

conductance of the magnons in the low-temperature limit. This effect has already been used in the study of bulk YIG to separate the contributions of magnons and phonons to the thermal conductivity by applying a large magnetic field [34–37].

We show in Fig. 4 the influence of the magnon-phonon coupling strength to the thermal conductance of the magnons. With the increase of the interacting strength, the magnon thermal conductance decreases and the peak moves to lower temperature. Obviously, a stronger coupling causes the magnons to be scattered by the phonons more strongly, and the magnon transport becomes less effective.

B. Thermal rectification and NDTC driven by magnon-phonon interaction

In this subsection, we consider the energy transfer between magnons and phonons at the FN interface. To do that, we introduce a large mismatch between the dynamical matrices and exchange coefficients of the left and right leads. Specifically, we choose a very large K_{ij}^L in the left lead and a very small exchange interaction J_{ij}^R in the right lead. This setting effectively blocks the pure phonon or magnon energy transport channel, and it makes the energy transfer between magnons and phonons the only transport channel at the interface. In this case, atom 2 actually becomes the interacting interface that allows the energy exchange between the magnons and phonons. A similar study of electron-phonon energy transfer at a metal-insulator junction has already been reported [19,30].

By applying a temperature difference between the left and right leads, we find TR and NDTC, as shown in Fig. 5. The dominant process that determines the thermal transport is the energy transfer between magnons and phonons at the interface. The efficiencies of the energy transfer are different for the two opposite processes at positive and negative temperature biases. For positive bias, heat flows from magnons to phonons, and the current grows monotonically with the temperature bias. For negative bias, there is a turning point for the NDTC at $\Delta T \approx 30$ K. This effect is larger for larger T_0.

The reason is as follows. Due to the presence of the magnetic field, there is a low-frequency gap in the magnon spectrum. The thermal excitation of the magnons has to overcome this extra energy. Thus, the magnons tend to "freeze" in the low-temperature range. This can be reflected from the local DOS projected onto the interface, which are defined by $\rho_2(\varepsilon) = -\frac{1}{\pi}\mathrm{Im}[G^r_{22}(\varepsilon)]$ for the magnons and $\nu_2(\omega) = -\frac{\hbar\omega}{\pi}\mathrm{Im}[D^r_{22}(\omega)]$ for the phonons [38], respectively, as shown in Fig. 6. To support this argument, we vary E_z to explore its influence on the energy current, as shown in Fig. 7. We can see in Fig. 7(b) that the lowest energy needed for the excitation of the magnons increases with the increase of the external magnetic field. With the decrease of the magnetic field, the energy current in the negative temperature bias increases greatly, and TR fades a lot, as seen in Fig. 7(a). So the TR and NDTD can be tuned

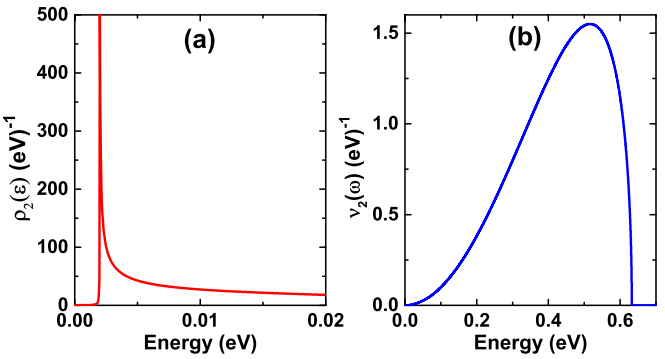

FIG. 6. Local density of states for (a) magnons and (b) phonons of atom 2. The parameters are the same with those of Fig. 5.

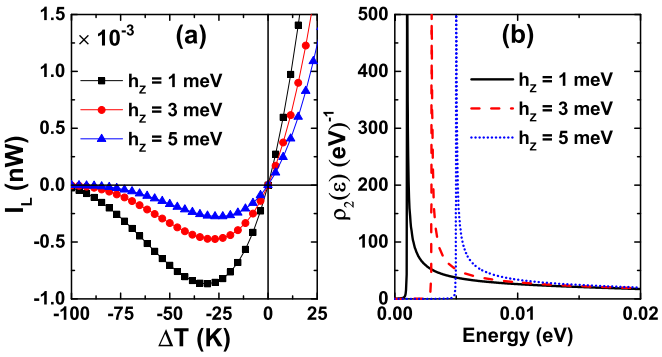

FIG. 7. (a) The energy current I_L as a function of the temperature bias. (b) The corresponding local density of states for the magnons of atom 2. The average temperature of the two electrodes is $T_0 = 60$ K. The other parameters are the same as those of Fig. 5.

effectively by the external magnetic field. This leads to the possibility of a magnetic-field-controlled thermal diode. This ability to control the TR is hard to realize in other similar setups using electron-phonon coupling [19,30], anharmonic phonon coupling [20], or asymmetric structures [39]. We note that the TR can also be realized in pure spin systems by smart control of the external magnetic field [40,41].

In real materials with an FN interface, the direct magnon-magnon and phonon-phonon transport channels may not be blocked abruptly, as we have assumed at the interface. To see the influence of this, we open the ballistic magnon channel gradually, i.e., we change J_{ij}^{R} and J_{23}^{CR} gradually until they are comparable to J_{ij}^{L}. As is shown in Fig. 8, when $J_{23}^{CR} = 0.05$ meV, still much smaller than J_{ij}^{L}, the total energy current I_L is almost linearly scaled with ΔT and is two orders of magnitude larger than $I_{J\to\mathrm{ph}}$, which implies that the ballistic transport becomes dominant. Similarly, in real materials, the phonon-phonon transport across the interface cannot be neglected. If $K_{ij}^{L} = K_{01}^{LC}$, and they are comparable to K_{23}^{CR}, with the other parameters not changed as those in Fig. 5, the ballistic phonon contribution to the energy current will be several orders of magnitude larger than that via the magnon-phonon channel. But for the magnon-phonon channel,

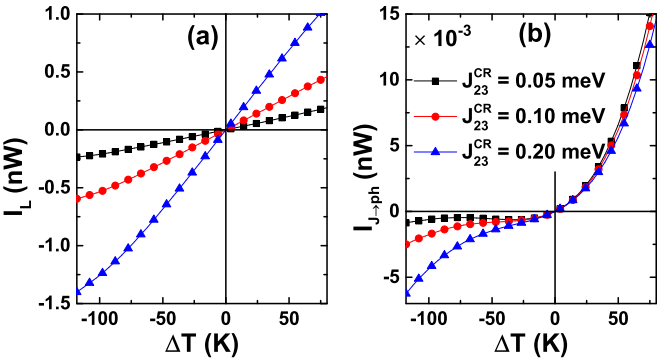

FIG. 8. (a) Total energy current out of the left lead. (b) Energy current via the magnon-phonon channel. We set $J_{23}^{CR} = J_{ij}^{R}$ and $h_z = 2$ meV for the whole region. The average temperature is $T_0 = 60$ K. The other parameters are the same as those of Fig. 5.

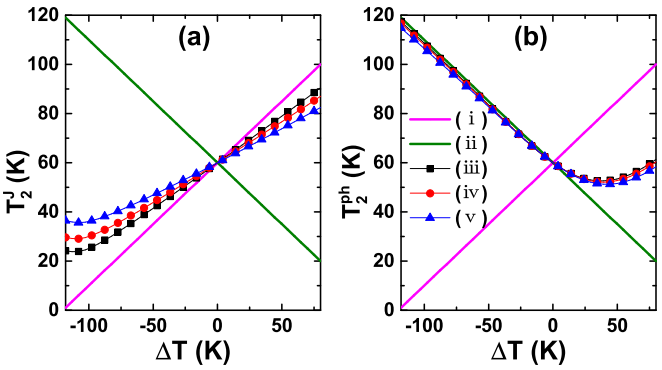

FIG. 9. Local temperatures for (a) magnons and (b) phonons of atom 2 as a function of the temperature bias. (i) Left lead temperature and (ii) Right lead temperature are given for comparison. (iii), (iv), and (v) correspond to the local temperatures of (a) magnons or (b) phonons with $J_{23}^{CR} = 0.05$, 0.1, and 0.2 meV, respectively. The other parameters are the same as in Fig. 8 except for the added probes. One probe is for measuring T_2^J and consists of a semi-infinite chain, with the exchange interaction $J_{ij}^{P} = 20$ meV in the lead. The other probe is for measuring T_2^{ph}, with the dynamic matrix element $K_{ij}^{P} = 2 \times 10^5$ meV^2. The two probes couple very weakly to the measured atom.

there are still TR and NDTC effects for small ballistic coupling J_{23}^{CR}, as shown in Fig. 8(b). However, when the coupling J_{23}^{CR} increases from 0.05 to 0.2 meV, the two effects fade gradually even for the magnon-phonon channel.

To explain this, we explore the effective local temperature of the interface. We use the Büttiker probes to "measure" the effective local temperature [42] of the magnons and phonons at the interface. The two temperatures are denoted as T_2^J and T_2^{ph}, respectively. The effective temperatures are determined when there is no heat flow between the probe leads and the atom probed.

We show in Fig. 9 the effective local temperatures for the magnons and phonons of the interface as a function of the temperature bias. By opening the ballistic magnon channel gradually, i.e., increasing the magnetic coupling strength of the interface to the right electrode from $J_{23}^{CR} = 0.05$ to 0.2 meV, the local magnon's temperature of the interface shifts toward the temperature of the right electrode, as shown in Fig. 9(a). The effective local temperature for the phonons of the interface has a similar but not obvious change in the negative temperature bias range, as shown in Fig. 9(b). However, in the positive temperature bias range, we note that it has an obvious nonmonotonic behavior with the increase of the temperature. The turning point is about $\Delta T \approx 40$ K. This is due to the hotter magnons, which pass energy to the colder phonons more efficiently via the magnon-phonon channel with the increase of the positive temperature bias, as can be seen clearly in Fig. 8(b). Similarly, in the large negative temperature bias, although the temperature of the left electrode decreases to the "freezing" temperature for the magnons, the local temperature for the magnons at the interface cannot get to the "freezing" temperature with the larger coupling strength, due to the ballistic magnon's heating effect from the hot right electrode. This leads to the disappearance of the TR and the NDTC in Fig. 8(b). So in order to build such an efficient thermal diode,

one needs to find efficient ways to suppress the ballistic thermal conductance of the phonons and magnons across the interface by using spectral mismatched materials.

IV. CONCLUSION

In summary, we study two cases of thermal transport of 1D systems with magnon-phonon interaction, one for a ferromagnetic-coupled junction and the other for an FN interface. In the former case, we show that the magnon-phonon interaction has a large influence on the magnon thermal conductance in the high-temperature range, while this is suppressed in the low-temperature range due to the external magnetic field. We note that this conclusion is qualitatively valid in ferromagnetic insulating crystals, where the spontaneous magnetization energy plays a role similar to the external magnetic field. For the case of the FN interface, we find TR and NDTC for the inelastic magnon-phonon channel. The effective local temperature imbalance between the local magnons and phonons at the interface together with the "freezing" effect of the external magnetic field play an important role in the two effects. External magnetic field control of the magnon spectrum is a unique feature of the magnon system, absent in purely phononic systems. For some bulk materials with the FN interface [10–12], or devices of molecule magnets [43,44], the pure phonon transport could be reduced a lot due to lattice mismatch or low-dimensional size, and the spin-phonon interaction could make the magnon-phonon transport channel a bottleneck for heat transfer at the interface. This could make the control of TR and NDTC possible and is useful for novel device applications.

ACKNOWLEDGMENT

We acknowledge the support by the National Natural Science Foundation of China (Grant No. 61371015).

APPENDIX: BALLISTIC THERMAL CONDUCTANCES FOR MAGNONS AND PHONONS IN A 1D CHAIN

The aim is to give a qualitative explanation to the quite different behavior of the thermal conductances of the magnons and phonons in the low-temperature limit in a ferromagnetic spin chain, where the magnon-phonon interaction is very weak due to the very limited thermal excitations and is thus omitted. It is convenient to demonstrate their different thermal conductances clearly by using a one-dimensional chain with translational invariance. In this case, the thermal conductances for the magnons and phonons can be written as

$$\kappa^i(T) = \int \frac{d\omega}{2\pi}\hbar\omega\mathcal{T}^i(\omega)\frac{\partial f^B(\omega,T)}{\partial T}, \tag{A1}$$

where $i = J,\mathrm{ph}$ for magnons and phonons, respectively. $f^B(\omega,T) = (e^{\frac{\hbar\omega}{k_BT}} - 1)^{-1}$ is the Bose distribution function, and the transmission function $\mathcal{T}^i(\omega)$ is

$$\mathcal{T}^J(\omega) = \begin{cases} 1, & h_z \leqslant \hbar\omega \leqslant h_z + 4J_0, \\ 0 & \text{otherwise} \end{cases} \tag{A2}$$

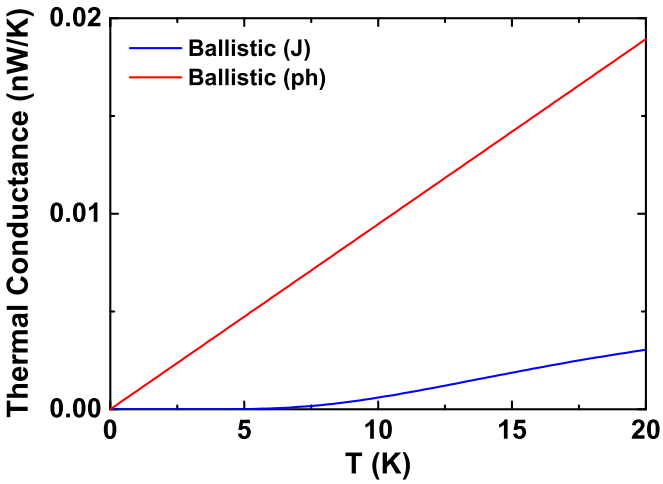

FIG. 10. Ballistic thermal conductances for magnons and phonons of a ferromagnetic spin chain under an external magnetic field in the low-temperature range. The magnetic field is $h_z = 4$ meV.

or

$$\mathcal{T}^{\mathrm{ph}}(\omega) = \begin{cases} 1, & 0 \leqslant \omega \leqslant 4\sqrt{K_0}, \\ 0 & \text{otherwise}, \end{cases} \tag{A3}$$

where J_0 is the nearest-neighbor Heisenberg exchange interaction, h_z is the magnetic energy due to the external field, and K_0 is the dynamic matrix element for the nearest-neighbor atoms. Equation (A1) can be written as

$$\kappa^i(T) = \int \frac{d\omega}{2\pi}\mathcal{T}^i(\omega)\frac{(\hbar\omega)^2 e^{\frac{\hbar\omega}{k_BT}}}{(e^{\frac{\hbar\omega}{k_BT}} - 1)^2 k_B T^2}. \tag{A4}$$

In the low-temperature limit, we assume $h_z, J_0, \hbar\sqrt{K_0} \gg k_BT$. We can simplify Eq. (A4) as

$$\begin{aligned}\kappa^J(T) &\approx \int_{h_z}^{+\infty} \frac{d\omega}{2\pi}\frac{(\hbar\omega)^2 e^{\frac{\hbar\omega}{k_BT}}}{(e^{\frac{\hbar\omega}{k_BT}} - 1)^2 k_B T^2} \\ &\approx \frac{h_z^2}{2\pi\hbar T} e^{-\frac{h_z}{k_BT}}\end{aligned} \tag{A5}$$

and

$$\begin{aligned}\kappa^{ph}(T) &\approx \int_0^{+\infty} \frac{d\omega}{2\pi}\frac{(\hbar\omega)^2 e^{\frac{\hbar\omega}{k_BT}}}{(e^{\frac{\hbar\omega}{k_BT}} - 1)^2 k_B T^2} \\ &= \frac{\pi k_B^2}{6\hbar} T.\end{aligned} \tag{A6}$$

We can see from Eqs. (A5) and (A6) that the ballistic magnon and phonon transport are quite different. For this special case, the phonon has a fully opening channel with a thermal conductance quantum showing a linear temperature dependence, but due to the gapped spectrum, magnons show an exponential dependence. We plot in Fig. 10 the ballistic thermal conductances for magnons and phonons given by Eqs. (A5) and (A6), respectively.

[1] G. E. Bauer, E. Saitoh, and B. J. van Wees, Nat. Mater. **11**, 391 (2012).

[2] K. Uchida, S. Takahashi, K. Harii, J. Ieda, W. Koshibae, K. Ando, S. Maekawa, and E. Saitoh, Nature (London) **455**, 778 (2008).

[3] K. Uchida, H. Adachi, T. Ota, H. Nakayama, S. Maekawa, and E. Saitoh, Appl. Phys. Lett. **97**, 172505 (2010).

[4] C. Jaworski, J. Yang, S. Mack, D. Awschalom, J. Heremans, and R. Myers, Nat. Mater. **9**, 898 (2010).

[5] C. Jaworski, R. Myers, E. Johnston-Halperin, and J. Heremans, Nature (London) **487**, 210 (2012).

[6] S. M. Wu, J. E. Pearson, and A. Bhattacharya, Phys. Rev. Lett. **114**, 186602 (2015).

[7] S. M. Wu, W. Zhang, Amit KC, P. Borisov, J. E. Pearson, J. S. Jiang, D. Lederman, A. Hoffmann, and A. Bhattacharya, Phys. Rev. Lett. **116**, 097204 (2016).

[8] J. Xiao, G. E. W. Bauer, K.-c. Uchida, E. Saitoh, and S. Maekawa, Phys. Rev. B **81**, 214418 (2010).

[9] H. Adachi, K. Uchida, E. Saitoh, J.-i. Ohe, S. Takahashi, and S. Maekawa, Appl. Phys. Lett. **97**, 252506 (2010).

[10] K. Uchida, H. Adachi, T. An, T. Ota, M. Toda, B. Hillebrands, S. Maekawa, and E. Saitoh, Nat. Mater. **10**, 737 (2011).

[11] K. Uchida, T. Ota, H. Adachi, J. Xiao, T. Nonaka, Y. Kajiwara, G. Bauer, S. Maekawa, and E. Saitoh, J. Appl. Phys. **111**, 103903 (2012).

[12] H. Adachi, K. Uchida, E. Saitoh, and S. Maekawa, Rep. Prog. Phys. **76**, 036501 (2013).

[13] M. Schreier, A. Kamra, M. Weiler, J. Xiao, G. E. W. Bauer, R. Gross, and S. T. B. Goennenwein, Phys. Rev. B **88**, 094410 (2013).

[14] I. Diniz and A. Costa, New J. Phys. **18**, 052002 (2016).

[15] B. Sothmann and M. Büttiker, Europhys. Lett. **99**, 27001 (2012).

[16] J. Ren and J.-X. Zhu, Phys. Rev. B **88**, 094427 (2013).

[17] J. Ren, J. Fransson, and J.-X. Zhu, Phys. Rev. B **89**, 214407 (2014).

[18] W. P. Su, J. R. Schrieffer, and A. J. Heeger, Phys. Rev. Lett. **42**, 1698 (1979).

[19] J. Ren and J.-X. Zhu, Phys. Rev. B **87**, 241412(R) (2013).

[20] B. Li, L. Wang, and G. Casati, Phys. Rev. Lett. **93**, 184301 (2004).

[21] N. Li, J. Ren, L. Wang, G. Zhang, P. Hänggi, and B. Li, Rev. Mod. Phys. **84**, 1045 (2012).

[22] J. T. Lü and J.-S. Wang, Phys. Rev. B **76**, 165418 (2007).

[23] J.-S. Wang, J. Wang, and J. T. Lü, Eur. Phys. J. B **62**, 381 (2008).

[24] T. Holstein and H. Primakoff, Phys. Rev. **58**, 1098 (1940).

[25] H. Haug and A.-P. Jauho, *Quantum Kinetics in Transport and Optics of Semiconductors* (Springer, Berlin, 1996).

[26] S. Datta, *Electronic Transport in Mesoscopic Systems* (Cambridge University Press, Cambridge, 1997).

[27] P. Hyldgaard, S. Hershfield, J. Davies, and J. Wilkins, Ann. Phys. (NY) **236**, 1 (1994).

[28] T. Frederiksen, M. Brandbyge, N. Lorente, and A.-P. Jauho, Phys. Rev. Lett. **93**, 256601 (2004).

[29] T. Frederiksen, M. Paulsson, M. Brandbyge, and A.-P. Jauho, Phys. Rev. B **75**, 205413 (2007).

[30] L. Zhang, J. T. Lü, J.-S. Wang, and B. Li, J. Phys.: Condens. Matter **25**, 445801 (2013).

[31] F. Mahfouzi and B. K. Nikolić, Phys. Rev. B **90**, 045115 (2014).

[32] Y. Meir and N. S. Wingreen, Phys. Rev. Lett. **68**, 2512 (1992).

[33] A.-P. Jauho, N. S. Wingreen, and Y. Meir, Phys. Rev. B **50**, 5528 (1994).

[34] J. E. Rives, G. S. Dixon, and D. Walton, J. Appl. Phys. **40**, 1555 (1969).

[35] D. J. Sanders and D. Walton, Phys. Rev. B **15**, 1489 (1977).

[36] S. R. Boona and J. P. Heremans, Phys. Rev. B **90**, 064421 (2014).

[37] S. M. Rezende and J. C. L. Ortiz, Phys. Rev. B **91**, 104416 (2015).

[38] W. Zhang, T. S. Fisher, and N. Mingo, Numer. Heat Transf., Pt. B **51**, 333 (2007).

[39] N. Yang, G. Zhang, and B. Li, Appl. Phys. Lett. **95**, 033107 (2009).

[40] K. A. van Hoogdalem and D. Loss, Phys. Rev. B **84**, 024402 (2011).

[41] D. Bagchi, J. Phys.: Condens. Matter **25**, 496006 (2013).

[42] J. Meair, J. P. Bergfield, C. A. Stafford, and Ph. Jacquod, Phys. Rev. B **90**, 035407 (2014).

[43] M. Ganzhorn, S. Klyatskaya, M. Ruben, and W. Wernsdorfer, Nat. Nanotechnol. **8**, 165 (2013).

[44] R. E. P. Winpenny, Nat. Nanotechnol. **8**, 159 (2013).